ExoMol line lists – XXII. The rotation-vibration spectrum of silane up to 1200 K

A. Owens,[1]⋆† A. Yachmenev,[2] W. Thiel,[3] J. Tennyson[1]⋆ and S. N. Yurchenko[1]⋆

[1] *Department of Physics and Astronomy, University College London, Gower Street, WC1E 6BT London, UK*
[2] *Center for Free-Electron Laser Science (CFEL), Deutsches Elektronen-Synchrotron DESY, Notkestrasse 85, D-22607 Hamburg, Germany*
[3] *Max-Planck-Institut für Kohlenforschung, Kaiser-Wilhelm-Platz 1, D-45470 Mülheim an der Ruhr, Germany*

ABSTRACT

A variationally computed $^{28}SiH_4$ rotation-vibration line list applicable for temperatures up to $T = 1200$ K is presented. The line list, called OY2T, considers transitions with rotational excitation up to $J = 42$ in the wavenumber range 0–5000 cm^{-1} (wavelengths $\lambda > 2$ μm). Just under 62.7 billion transitions have been calculated between 6.1 million energy levels. Rovibrational calculations have utilized a new 'spectroscopic' potential energy surface determined by empirical refinement to 1452 experimentally derived energy levels up to $J = 6$, and a previously reported *ab initio* dipole moment surface. The temperature-dependent partition function of silane, the OY2T line list format, and the temperature dependence of the OY2T line list are discussed. Comparisons with the PNNL spectral library and other experimental sources indicate that the OY2T line list is robust and able to accurately reproduce weaker intensity features. The full line list is available from the ExoMol data base and the CDS data base.

Key words: molecular data – opacity – planets and satellites: atmospheres – stars: atmospheres – ISM: molecules.

1 INTRODUCTION

The possibility of silicon-based life existing elsewhere in the Universe is an idea very much rooted in the realms of science fiction. Yet the continued discovery of exoplanets and the exhaustive search for potential biosignature gases (Seager, Bains & Petkowski 2016) has renewed interest in the simplest silicon-hydrogen compound, silane (SiH$_4$). A large number of high-resolution studies on the infrared (IR) absorption spectrum of SiH$_4$ and its isotopomers have been reported since the first measurements by Steward & Nielsen (1934, 1935). Rotation-vibration transitions have been detected around the carbon star IRC +10216 (Goldhaber & Betz 1984; Keady & Ridgway 1993; Monnier et al. 2000), and in the atmospheres of Jupiter (Treffers et al. 1978) and Saturn (Larson et al. 1980). Although deemed unlikely, silane has already been considered in the context of H$_2$-dominated atmospheres on rocky exoplanets (Seager, Bains & Hu 2013).

Despite efforts to document the spectrum of SiH$_4$, no complete line list exists for this molecule. The PNNL spectral library (Sharpe et al. 2004) contains IR absorption cross-sections at a reso-

lution of around 0.06 cm^{-1} for the 600–6500 cm^{-1} range. Another useful resource is the Spherical Top Data System (STDS; Wenger & Champion 1998), however, a significant portion of the measured transitions and intensities are from unpublished work which makes it difficult to assess the reliability of the data. Theoretical $^{28}SiH_4$ spectra are available from the TheoReTS data base (Rey et al. 2016) for a temperature range of 70–300 K but the calculations that they are based on are again from unpublished work. A room temperature line list has been produced for the 750–1150 cm^{-1} region from analysis of the ν_2 and ν_4 bands (Ulenikov et al. 2017). Whilst absolute line intensities have been determined by van Helden et al. (2015) for a large number of P-branch transitions of the ν_3 band up to the rotational quantum number $J = 16$.

Previously, we generated potential energy and dipole moment surfaces for silane using state-of-the-art *ab initio* theory (Owens et al. 2015). Both surfaces were rigorously evaluated and showed good agreement with experimental results. Computed fundamental term values of $^{28}SiH_4$ using the CBS-F12^{HL} potential energy surface (PES) possessed a root-mean-square (rms) error of 0.63 cm^{-1} compared to experiment. The dipole moment surface (DMS), although tending to marginally overestimate the strength of line intensities, reproduced band shape and structure well.

Building on this work, we present a comprehensive rotation-vibration line list of $^{28}SiH_4$ suitable for elevated temperatures. The line list, called OY2T, has been computed variationally and utilizes a new 'spectroscopic' PES which has been determined by

⋆ E-mail: alec.owens@cfel.de (AO); j.tennyson@ucl.ac.uk (JT); s.yurchenko@ucl.ac.uk (SNY)
† Present address: The Hamburg Center for Ultrafast Imaging, Universität Hamburg, Luruper Chaussee 149, 22761 Hamburg, Germany.

rigorous empirical refinement. The OY2T line list has been produced for the ExoMol data base (Tennyson & Yurchenko 2012; Tennyson et al. 2016), which is providing important molecular spectroscopic data to help characterize exoplanet and other hot atmospheres. Examples of the application of these line lists include: the early detection of water in HD 189733b (Tinetti et al. 2007) and HD 209458b (Beaulieu et al. 2010) using the BT2 line list (Barber et al. 2006); the tentative identification of HCN in the atmosphere of super-Earth 55 Cancri e (Tsiaras et al. 2016) and TiO in the atmosphere of hot Jupiter WASP-76 b (Tsiaras et al. 2017); various studies using the 10to10 line list (Yurchenko & Tennyson 2014) to detect methane in exoplanets (Beaulieu et al. 2011; Yurchenko et al. 2014; Tsiaras et al. 2017), the bright T4.5 brown dwarf 2MASS 0559-14 (Yurchenko et al. 2014), and to make detailed line assignments in the near-infrared spectra of late T dwarfs (Canty et al. 2015) in conjunction with the BYTe ammonia line list (Yurchenko, Barber & Tennyson 2011). Conversely, a line list for the diatomic NaH molecule (Rivlin et al. 2015) was able to rule out the tentative detection of this species in the atmosphere of a brown dwarf.

Silane is the second five-atom molecule to be treated within the ExoMol framework (Tennyson & Yurchenko 2017) after methane and the 10to10 line list (Yurchenko & Tennyson 2014), which demonstrated the need to consider a very large number of transitions to correctly model the opacity at elevated temperatures (Yurchenko et al. 2014). Since the 10to10 line list, several key developments have taken place in our nuclear motion code TROVE (Yurchenko, Thiel & Jensen 2007; Yachmenev & Yurchenko 2015) that significantly ease the computational burden of theoretical line list production. These include an automatic differentiation method to construct the rovibrational Hamiltonian, the implementation of curvilinear internal coordinates and a novel vibrational basis set truncation approach which will be discussed later on.

The paper is structured as follows: In Section 2 we detail the empirical refinement of the CBS-F12^{HL} PES, the DMS and intensity simulations and the variational calculations. In Section 3, the OY2T line list is presented and we discuss the temperature-dependent partition function of SiH$_4$, the format of the OY2T line list, the temperature dependence of the OY2T line list and comparisons with the PNNL spectral library and other experimental data. Concluding remarks are given in Section 4.

2 METHODS

2.1 Potential energy surface refinement

The CBS-F12^{HL} PES (Owens et al. 2015) was constructed from extensive, explicitly correlated coupled cluster calculations with extrapolation to the complete basis set limit, and incorporated additional higher-level energy corrections to account for core-valence electron correlation, higher-order coupled cluster terms beyond CCSD(T) and scalar relativistic effects. Although impressive in its accuracy, orders-of-magnitude improvements in predicted transition frequencies can be achieved by refining the PES to experiment. Furthermore, improved energy levels means better wavefunctions and more reliable intensities.

The refinement was carried out using an efficient least-squares fitting procedure (Yurchenko et al. 2011) implemented in TROVE. The procedure works by assuming the CBS-F12^{HL} PES, $V_{CBS-F12^{HL}}$, is already a reasonable representation such that the effect of the refinement can be treated as a perturbation ΔV, i.e.
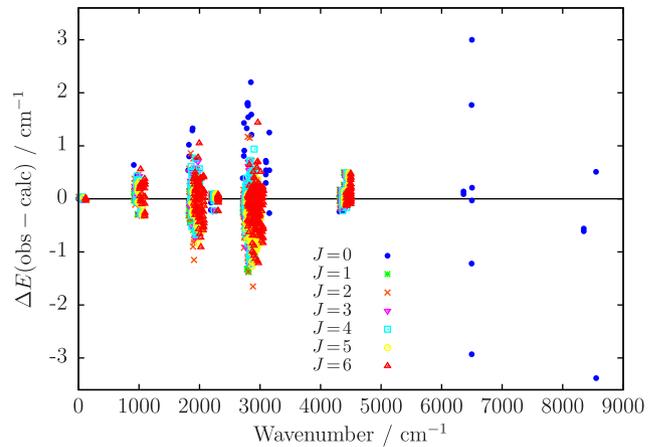
$$V' = V_{CBS-F12^{HL}} + \Delta V, \qquad (1)$$

Figure 1. Fitting residuals, $\Delta E(\text{obs-calc}) = E_{obs} - E_{calc}$, of the 1452 energy levels used in the PES refinement.

where V' is the refined PES. The correction ΔV is expanded in terms of nine vibrational coordinates $\boldsymbol{\xi} = \{\xi_1, \xi_2, \ldots, \xi_9\}$ according to the formula,

$$\Delta V = \sum_{ijk\ldots} \Delta f_{ijk\ldots} \left\{ \xi_1^i \xi_2^j \xi_3^k \ldots \right\}^{A_1}, \qquad (2)$$

where the coefficients $\Delta f_{ijk\ldots}$ are corrections to the original PES expansion parameters $f_{ijk\ldots}$. The expansion terms $\{\xi_1^i \xi_2^j \xi_3^k \ldots\}^{A_1}$ are symmetrized combinations of the vibrational coordinates $\boldsymbol{\xi} = \{\xi_1, \xi_2, \ldots, \xi_9\}$ and transform according to the A_1 irreducible representation of the $\boldsymbol{T}_d(M)$ molecular symmetry group (Bunker & Jensen 1998). Further details on the vibrational coordinates and analytic representation of the CBS-F12^{HL} PES can be found in Owens et al. (2015).

The new perturbed Hamiltonian, $H' = H + \Delta V$, is then diagonalized using a basis set of eigenfunctions from the initial unperturbed Hamiltonian H eigenvalue problem. Each iteration utilizes the previous 'unperturbed' basis set in this way until a PES of desirable quality is reached. To ensure the consistency of the refined surface, the expansion parameters $f_{ijk\ldots}$ are simultaneously fitted to both the experimental data and the original *ab initio* data set (Yurchenko et al. 2003). This stops any unrealistic distortion of the PES in regions not sampled by experiment. It also means each expansion parameter can be adjusted irrespective of the amount, or distribution, of experimental energies used in the refinement.

For SiH$_4$, a total of 1452 experimental term values up to $J = 6$ were used to refine the CBS-F12^{HL} PES. This included 53 vibrational $J = 0$ band centres from Wenger & Champion (1998), Chevalier (1988), Zhu et al. (1991), Sun et al. (1995) and Lin et al. (1998), and 1399 $J > 0$ energies from the STDS (Wenger & Champion 1998). Of the 106 expansion parameters of the CBS-F12^{HL} PES, 104 were varied and the results of the refinement are shown in Fig. 1, where we have plotted the fitting residuals $\Delta E(\text{obs-calc}) = E_{obs} - E_{calc}$. Here, E_{obs} and E_{calc} are the observed and calculated energies, respectively. Overall, the experimental energy levels are reproduced with an rms error of 0.454 cm^{-1}. This error is slightly larger than what is achievable with refinement, however, this was intentional. The energy levels from the STDS are derived from an effective Hamiltonian model based on some unpublished work. It is therefore hard to assess the reliability of the data and how much it can be trusted in the refinement. Despite this, because the CBS-F12^{HL} PES is reliable we could depend on it

more and ensure the refined PES did not deviate too far away from the original surface.

Pure rotational energies were given the largest weights in the refinement, while $J = 0$ and rovibrational term values were weighted two orders of magnitude smaller with values between 1–10 based on their energy. Since the weights are normalized in the fitting, relative weighting is more important than absolute values (see Yurchenko et al. 2011 for further details). Although we have determined a new 'spectroscopic' PES of silane, the accuracy of the refined PES is only guaranteed with the computational setup employed in this study. This is usually the case in theoretical line list production using programs that do not treat the kinetic energy operator exactly, and we therefore do not recommend this PES for use otherwise.

2.2 Dipole moment surface and line intensities

The electric DMS utilized for the present study was computed at the CCSD(T)/aug-cc-pVTZ(+d for Si) level of theory. Further details on the analytic representation and performance of the DMS can be found in Owens et al. (2015), where it was shown that the DMS marginally overestimates the strength of line intensities. This discrepancy is very minor though as we will see in Section 3.3.

To simulate absolute absorption intensities we used the expression,

$$I(f \leftarrow i) = \frac{A_{if}}{8\pi c} g_{ns}(2J_f + 1) \frac{\exp(-E_i/kT)}{Q(T)\, \nu_{if}^2}$$
$$\times \left[1 - \exp\left(-\frac{hc\nu_{if}}{kT} \right) \right], \tag{3}$$

where A_{if} is the Einstein A coefficient of a transition with wavenumber ν_{if} (in cm^{-1}) between an initial state with energy E_i, and a final state with rotational quantum number J_f. Here, k is the Boltzmann constant, T is the absolute temperature, h is the Planck constant and c is the speed of light. The nuclear spin statistical weights are $g_{ns} = \{5, 5, 2, 3, 3\}$ for states of symmetry $\{A_1, A_2, E, F_1, F_2\}$, respectively. The partition function for a given temperature $Q(T)$ will be discussed in Section 3.1. All transitions obey the symmetry selection rules

$$A_1 \leftrightarrow A_2, \ E \leftrightarrow E, \ F_1 \leftrightarrow F_2, \tag{4}$$

and the standard rotational selection rules,

$$J' - J'' = 0, \pm 1, \ J' + J'' \neq 0, \tag{5}$$

where $'$ and $''$ denote the upper and lower state, respectively. Note that the EXOCROSS code (Yurchenko, Al-Refaie & Tennyson, in preparation; available at http://www.exomol.com/software/) was employed for all spectral simulations.

2.3 Variational calculations

The computer program TROVE was used for all rovibrational calculations. Since the methodology of TROVE is well documented (Yurchenko, Thiel & Jensen 2007; Yurchenko et al. 2009; Yachmenev & Yurchenko 2015; Yurchenko, Yachmenev & Ovsyannikov 2017) and we have previously reported calculations on SiH$_4$ (Owens et al. 2015), we summarize only the key aspects relevant for this work.

The rovibrational Hamiltonian was constructed numerically using an automatic differentiation method (Yachmenev & Yurchenko 2015). The Hamiltonian was represented as a power series expansion around the equilibrium geometry in terms of nine,

curvilinear internal coordinates, with the kinetic and potential energy operators truncated at 6th order. Atomic mass values were used throughout. A multistep contraction scheme was used to build the vibrational basis set, the size of which was controlled by the polyad number

$$P = 2(n_1 + n_2 + n_3 + n_4) + n_5 + n_6 + n_7 + n_8 + n_9 \leq P_{\max}. \tag{6}$$

The quantum numbers n_k for $k = 1, \ldots, 9$ are related to primitive basis functions ϕ_{n_k}, which are obtained by solving a one-dimensional Schrödinger equation for each kth vibrational mode with the Numerov–Cooley method (Noumerov 1924; Cooley 1961). Multiplication with symmetrized rigid-rotor eigenfunctions $|J, \Gamma_{rot}, n\rangle$ produces the final basis set for $J > 0$ calculations. Here, the label Γ_{rot} is the rotational symmetry and n is a multiplicity index used to count states within a given J (see Boudon et al. 2006).

In calculations we set $P_{\max} = 12$, which resulted in 19 237 vibrational basis functions corresponding to energies up to $hc \cdot 15\,000$ cm^{-1}. Describing high rotational excitations with such a large basis set can quickly become computationally intractable (rovibrational matrices scale linearly with J). It was therefore necessary to reduce the number of basis functions. To do this we employed a new, basis set truncation approach (Yurchenko et al., in preparation) based on vibrational transition moments, which are relatively inexpensive to compute in TROVE. The vibrational transition moment between two states is defined as,

$$\mu_{if} = \sqrt{\sum_{\alpha = x, y, z} |\langle \Phi_{vib}^{(f)} | \bar{\mu}_\alpha | \Phi_{vib}^{(i)} \rangle|^2}, \tag{7}$$

where $|\Phi_{vib}^{(i)}\rangle$ and $|\Phi_{vib}^{(f)}\rangle$ are the initial and final state vibrational eigenfunctions, respectively, and $\bar{\mu}_\alpha$ is the electronically averaged dipole moment function along the molecule-fixed axis $\alpha = x, y, z$.

After computing $J = 0$ energies, all possible transition moments were calculated for a lower energy threshold of $hc \cdot 8000$ cm^{-1} (same as for the final OY2T line list). Once known, we estimated the vibrational band intensity at an elevated temperature (e.g. 1500 K) for every transition moment. Each vibrational energy level, and consequently each $J = 0$ basis function, was assigned a band intensity value which was simply the largest computed for that state when acting as $|\Phi_{vib}^{(i)}\rangle$ in equation (7). The $J = 0$ basis set was then pruned by removing basis functions and energy levels above $hc \cdot 8000$ cm^{-1} with band intensity values smaller than 1×10^{-21} cm molecule^{-1}. This is around three orders of magnitude smaller than the largest computed value. The band intensity threshold was chosen solely on a computational basis so that the rovibrational calculations were manageable with the resources available to us. The resulting pruned basis set contained 3817 functions (corresponding to energies up to $hc \cdot 15\,000$ cm^{-1}) and was multiplied in the usual manner with symmetrized rigid-rotor functions for $J > 0$ calculations.

An advantage of this truncation approach is that the accuracy of the vibrational energy levels and respective wavefunctions computed using a larger value of $P_{\max}$ is retained. Naturally, we will lose some information on weaker lines involving states above $hc \cdot 8000$ cm^{-1} and it is hard to quantify the effect without more rigorous calculations. Removing functions from the basis set will also influence predicted rovibrational energies but the errors introduced, and the basis set convergence error, can to some extent be compensated for by refining the PES with the pruned basis set, which is what we have done. The resulting 'effective' PES is only reliable with the same computational setup but this is usually the case in theoretical line list production with TROVE.

Table 1. Vibrational modes of SiH$_4$ and the observed band centres (in cm^{-1}) from Wenger & Champion (1998).

Mode	Symmetry	Band centre	Description
ν_1	A_1	2186.87	Symmetric stretching
ν_2	E	970.93	Antisymmetric bending
ν_3	F_2	2189.19	Antisymmetric stretching
ν_4	F_2	913.47	Antisymmetric bending
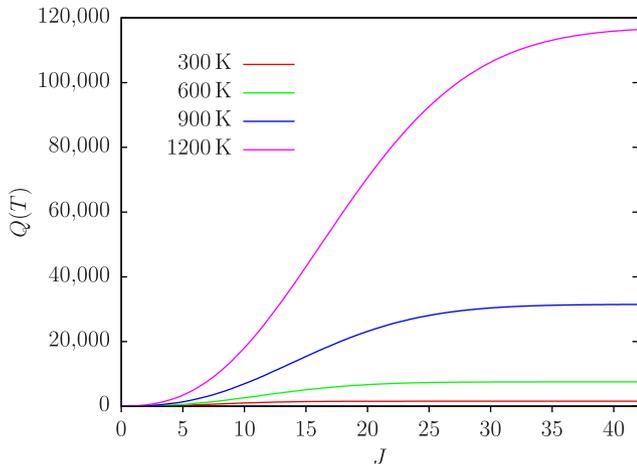
Figure 2. Convergence of the partition function $Q(T)$ with respect to the rotational quantum number J for different temperatures.

The OY2T line list was computed with a lower state energy threshold of $hc \cdot 8000\,\text{cm}^{-1}$ and considered transitions up to $J = 42$ in the 0–5000 cm^{-1} range. To improve the accuracy of the line list we employed an empirical basis set correction (EBSC; Yurchenko et al. 2009), which is essentially a shift of the band centres to better match experiment. Recall that in the multistep contraction scheme used by TROVE, the $J = 0$ eigenfunctions form the final basis set and the vibrational part of the Hamiltonian is diagonal with respect to this basis set. It is possible then to replace the diagonal elements with accurate experimental values for the $J = 0$ energies when constructing the Hamiltonian matrix. For the OY2T line list, only the four fundamentals, listed in Table 1, were replaced as these wavenumbers are well established.

3 RESULTS

3.1 Partition function of silane

The temperature-dependent partition function $Q(T)$ is defined as,

$$Q(T) = \sum_i g_i \exp\left(-\frac{E_i}{kT}\right), \qquad (8)$$

where $g_i = g_{\text{ns}}(2J_i + 1)$ is the degeneracy of a state i with energy E_i and rotational quantum number J_i. Summing over all computed rovibrational energy levels, in Fig. 2 we have plotted the convergence of $Q(T)$ as a function of J for different temperatures. At $T = 1200\,\text{K}$ the partition function is converged to around 0.1 per cent. Our calculated room temperature partition function $Q(296\,\text{K}) = 1532.93$ is in excellent agreement with a value of $Q(296\,\text{K}) = 1533.00$ from the TheoReTS data base (Rey et al. 2016). It also agrees well with an approximate estimate of $Q \approx Q_{\text{rot}} \times Q_{\text{vib}} = 1527.36$ used in our previous study (Owens et al. 2015), where Q_{rot} and Q_{vib} are the rotational and vibrational partition function, respectively.
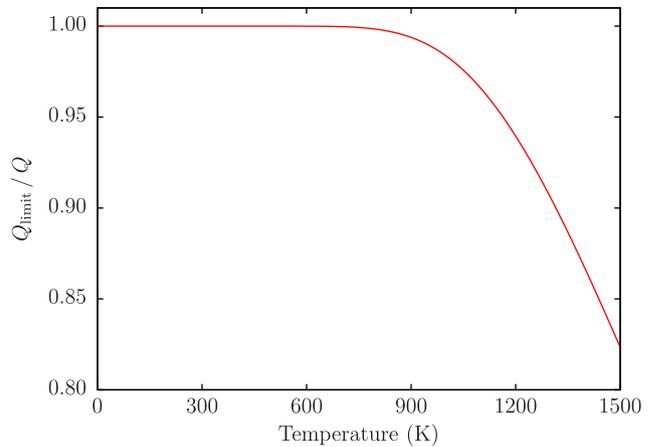
Figure 3. Plot of the ratio Q_{limit}/Q as a function of temperature. This ratio provides a measure of completeness for the OY2T line list.

Given that the OY2T line list has been computed with a lower energy threshold of $hc \cdot 8000\,\text{cm}^{-1}$, it is informative to study a reduced partition function Q_{limit}, which only considers energy levels up to $hc \cdot 8000\,\text{cm}^{-1}$ in the summation of equation (8). In Fig. 3 we plot the ratio Q_{limit}/Q with respect to temperature, and this can provide a measure of completeness of the OY2T line list. At $T = 1200\,\text{K}$, the ratio $Q_{\text{limit}}/Q = 0.94$, and we recommend this as a 'soft' temperature limit to the OY2T line list. Using the line list above this temperature will result in the progressive loss of opacity, however, it is possible to estimate the missing contribution with the ratio Q_{limit}/Q (Neale, Miller & Tennyson 1996). Note that our full partition function evaluated on a 1 K grid from 70–1400 K is provided as supplementary material.

3.2 OY2T line list format

A complete description of the ExoMol data structure along with examples was recently reported by Tennyson et al. (2016). The .states file contains all computed rovibrational energies (in cm^{-1}). Each energy level possesses a unique state ID with symmetry and quantum number labelling as shown in Table 2. The .trans files, which are split into frequency windows so that they are easier to handle, contain all computed transitions with upper and lower state ID labels, and Einstein A coefficients. An example from a .trans file for the OY2T line list is given in Table 3.

3.3 Validation of the OY2T line list

The OY2T line list contains nearly 62.7 billion (62 690 449 078) transitions between 6.1 million (6 142 521) energy levels. The distribution of lines and energies is illustrated in Fig. 4, where we have plotted the total number computed for each value of J. The density of transitions is largest between $18 \leq J \leq 26$ but this drops off relatively smoothly and by $J = 42$, we have nearly calculated all possible transitions for our computational setup (e.g. lower energy threshold of $hc \cdot 8000\,\text{cm}^{-1}$, wavenumber range of 5000 cm^{-1}, pruned rovibrational basis set, etc.). The decrease in the number of energy levels after $J = 34$ is a result of the upper energy threshold of $hc \cdot 13{,}000\,\text{cm}^{-1}$

The temperature dependence of the OY2T line list is shown in Fig. 5, where we have simulated integrated absorption

Table 2. Extract from the `.states` file for the OY2T line list.

| N	$\tilde{E}$	g_{tot}	J	Γ_{tot}	n_1	n_2	n_3	n_4	n_5	n_6	n_7	n_8	n_9	Γ_{vib}	J	K	τ_{rot}	Γ_{rot}	$|C_i^2|$
1	0.000000	5	0	1	0	0	0	0	0	0	0	0	0	1	0	0	0	1	0.99
2	1810.753814	5	0	1	0	0	0	0	0	0	2	0	0	1	0	0	0	1	0.32
3	1936.931391	5	0	1	0	0	0	0	2	0	0	0	0	1	0	0	0	1	0.49
4	2186.873254	5	0	1	0	0	1	0	0	0	0	0	0	1	0	0	0	1	0.24
5	2730.476494	5	0	1	0	0	0	0	0	0	1	1	1	1	0	0	0	1	0.91
6	2792.635361	5	0	1	0	0	0	0	1	0	2	0	0	1	0	0	0	1	0.49
7	2914.995074	5	0	1	0	0	0	0	1	2	0	0	0	1	0	0	0	1	0.73
8	3099.093127	5	0	1	0	0	1	0	0	0	0	0	1	1	0	0	0	1	0.69
9	3599.518736	5	0	1	0	0	0	0	0	0	2	0	2	1	0	0	0	1	0.20
10	3651.898227	5	0	1	0	0	0	0	0	0	0	4	0	1	0	0	0	1	0.21

N: State ID;

$\tilde{E}$: Term value (in cm^{-1});

g_{tot}: Total degeneracy;

J: Rotational quantum number;

Γ_{tot}: Total symmetry in $\boldsymbol{T}_d(M)$ (1 is A_1, 2 is A_2, 3 is E, 4 is F_1, 5 is F_2);

$n_1 - n_9$: TROVE vibrational quantum numbers;

Γ_{vib}: Symmetry of the vibrational contribution in $\boldsymbol{T}_d(M)$;

J: Rotational quantum number (same as column 4);

K: Rotational quantum number, projection of J on to molecule-fixed z-axis;

τ_{rot}: Rotational parity (0 or 1);

Γ_{rot}: Symmetry of the rotational contribution in $\boldsymbol{T}_d(M)$;

$|C_i^2|$: Largest coefficient used in the assignment.

Table 3. Extract from the `.trans` file for the OY2T line list.

f	i	A_{if}
1009016	887497	2.8705e-05
1012938	889497	1.6387e-05
1013144	1138036	5.4460e-02
1013796	1138422	1.0351e-01
101385	61971	5.4116e-04
1014053	890062	1.6747e-04
1014363	1010642	4.0593e-03
1016000	1139649	5.9798e-02
1017478	892208	1.0542e-06
1017606	1140576	5.3820e-03

f: Upper state ID; i: Lower state ID;

A_{if}: Einstein A coefficient (in s^{-1}).

cross-sections at a resolution of $1\,\text{cm}^{-1}$ using a Gaussian profile with a half width at half-maximum (hwhm) of $1\,\text{cm}^{-1}$. Very weak intensities can be seen to grow several orders of magnitude stronger as the temperature increases. This smoothing of the spectrum is a result of vibrationally excited states becoming more populated and causing the rotational band envelope to broaden.

A good benchmark of the OY2T line list is to compare with the PNNL spectral library (Sharpe et al. 2004). In Figs 6 and 7, we have simulated cross-sections at a resolution of $0.06\,\text{cm}^{-1}$ using a Gaussian profile with a hwhm of $0.135\,\text{cm}^{-1}$. The experimental PNNL silane spectrum was measured at a temperature of $25\,^{\circ}\text{C}$ with the data set subsequently re-normalized to $22.84\,^{\circ}\text{C}$ (296 K). It is of electronics grade silane gas, which is composed of ^{28}SiH$_4$ (92.2 per cent), ^{29}SiH$_4$ (4.7 per cent) and ^{30}SiH$_4$ (3.1 per cent). We have therefore scaled our computed ^{28}SiH$_4$ cross-sections by 0.922 to ensure a reliable comparison. As expected (Owens et al. 2015), the OY2T cross-sections are marginally stronger but this is very
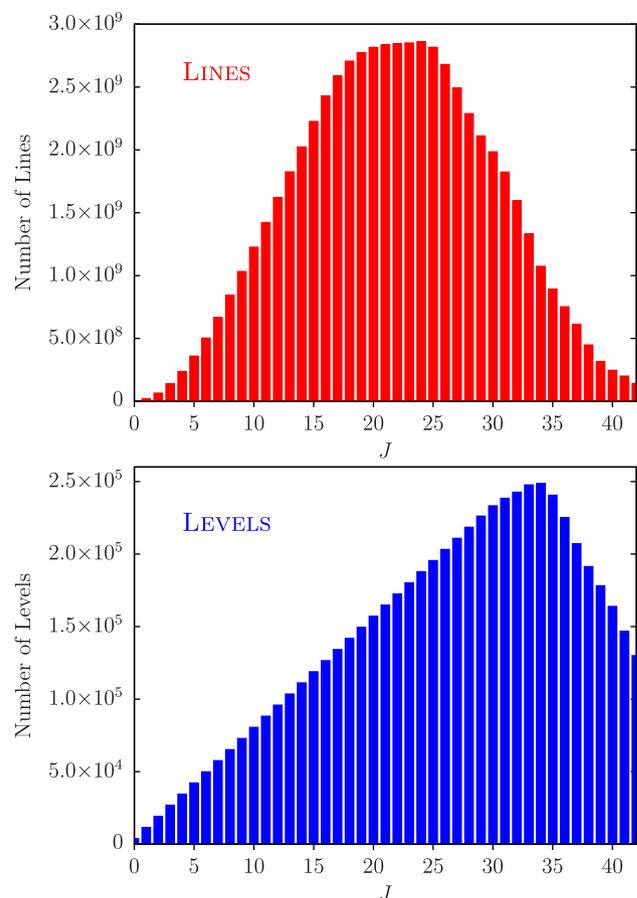
Figure 4. The number of lines and energy levels in the OY2T line list for each value of the rotational quantum number J.
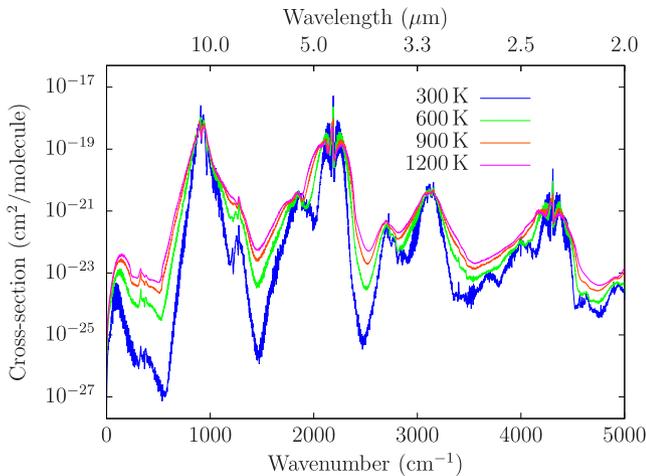
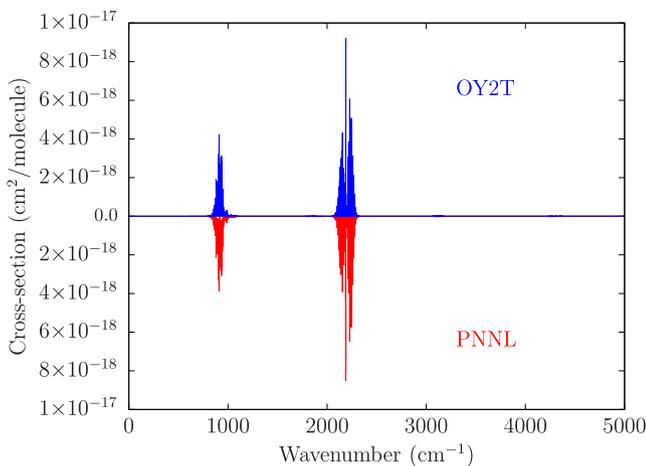**Figure 5.** Temperature dependence of the OY2T line list.

Figure 6. Overview of OY2T cross-sections compared with the PNNL spectral library at $T = 296$ K. Note that the experimental PNNL spectrum (Sharpe et al. 2004) is composed of $^{28}SiH_4$ (92.2 per cent), $^{29}SiH_4$ (4.7 per cent), and $^{30}SiH_4$ (3.1 per cent) (see text).

slight. Overall the agreement is very encouraging, particularly the performance of the OY2T line list for weaker bands (see the right-hand panels of Fig. 7) as we are missing contributions from $^{29}SiH_4$ and $^{30}SiH_4$.

Finally, we compare absolute line intensities of the OY2T line list with measurements of the ν_3 band from van Helden et al. (2015), and with the 750–1150 cm^{-1} region line list from Ulenikov et al. (2017). Intensities were computed using equation (3) at $T = 296$ K in Fig. 8, and at $T = 298$ K in Fig. 9. As was previously found when validating the DMS (Owens et al. 2015), there is good agreement with the results of van Helden et al. (2015), where transition intensities up to $J = 16$ were recorded at a resolution of 0.0011 cm^{-1} with an estimated experimental measurement accuracy of 10 per cent. For the $^{28}SiH_4$ line list from Ulenikov et al. (2017) the agreement is also pleasing. Their line list contains 3512 transitions up to $J = 27$ with the intensities determined from an analysis of 787 of the measured lines. Again the OY2T line intensities are slightly stronger in places but overall the band structure is well matched and weaker intensity features are accurately accounted for. It is worth noting that the

OY2T line list is up to $J = 42$ which would explain some of the additional spectral features in both comparisons.

4 CONCLUSION

A comprehensive rotation-vibration line list for $^{28}SiH_4$ has been presented. The OY2T line list covers the 0–5000 cm^{-1} region and includes transitions up to $J = 42$. Analysis of the temperature-dependent partition function suggests that the OY2T line list can be confidently used for temperatures below $T = 1200$ K. Applications above this temperature are likely to result in the loss of opacity. Comparisons with the PNNL spectral library and other experimental sources showed that the OY2T line list is robust and able to accurately reproduce the intensity features of weaker bands. The OY2T line list can be downloaded from the ExoMol data base at www.exomol.com or the CDS data base at http://cdsarc.u-strasbg.fr.

The OY2T line list will be useful for modelling the absorption of SiH$_4$ in the atmospheres of exoplanets. Its quality (completeness and accuracy) should be sufficient, at least in principle, to detect silane in the atmosphere of a hot exoplanet from transit spectroscopic observations when combined with a proper atmospheric and radiative transfer model (assuming the abundance of SiH$_4$ is large enough to be detected). However for high resolution detection techniques such as the high-dispersion spectroscopy developed by Snellen (2014), our line positions may not be sufficiently accurate. This technique is based on the Doppler shifts of a large number of spectroscopic lines of a given species, which are cross-correlated to reference lab data on the line positions. The required resolution of the line positions should be as high as, $R \geq 100\,000$. We have a method to address this problem, which is to replace the theoretical energy levels in a synthetic line list with experimentally derived ones, usually obtained with the measured active rotational-vibrational energy levels (MARVEL) procedure (Furtenbacher, Császár & Tennyson 2007; Furtenbacher & Császár 2012). The most recent example of this is the hybrid line list for H$_3^+$ MiZATeP (Mizus et al. 2017). The experimental spectroscopic data available for SiH$_4$ should be sufficient to generate such a hybrid line list for this molecule in the future.

Natural extensions to the OY2T line list would be the consideration of a larger frequency range, an increased lower energy threshold in computations and the inclusion of higher rotational excitations. These issues, although computationally challenging, are straightforward to address but will only be done if there is a demand for such work. It would be useful to derive a consistent set of normal mode quantum numbers v_k for the OY2T line list. These are commonly used in high-resolution spectroscopic applications and could be easily incorporated by updating the .states file. Work in this direction is underway and any updates to the OY2T line list will be released on the ExoMol website. It may also be worthwhile to explore a more compact representation (Yurchenko et al. 2017) of the OY2T line list given the huge number of lines that have been generated. Certainly we are in a position to produce temperature-dependent cross-sections for a fixed resolution if requested.
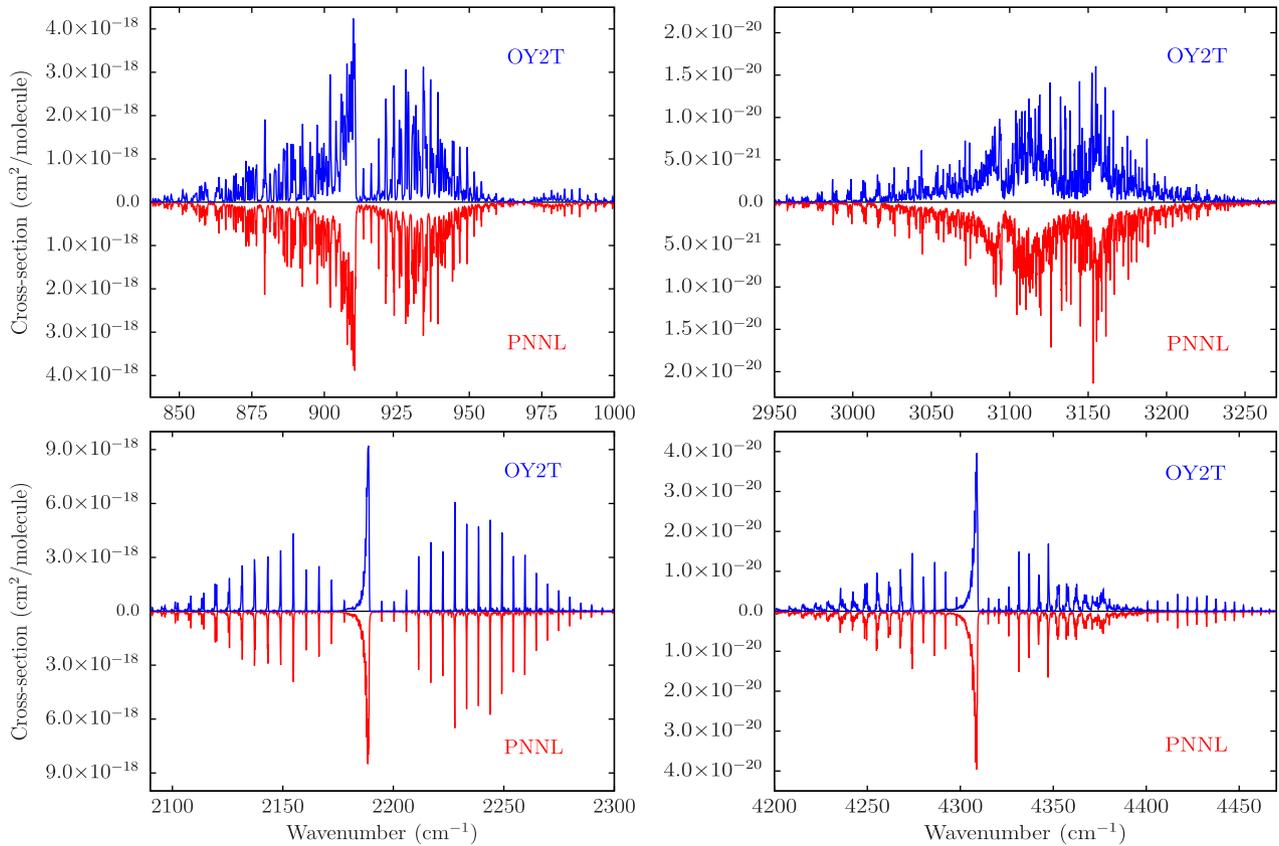
Figure 7. Closer inspection of OY2T cross-sections compared with the PNNL spectral library at $T = 296$ K. Note that the experimental PNNL spectrum (Sharpe et al. 2004) is composed of ^{28}SiH$_4$ (92.2 per cent), ^{29}SiH$_4$ (4.7 per cent) and ^{30}SiH$_4$ (3.1 per cent) (see text).
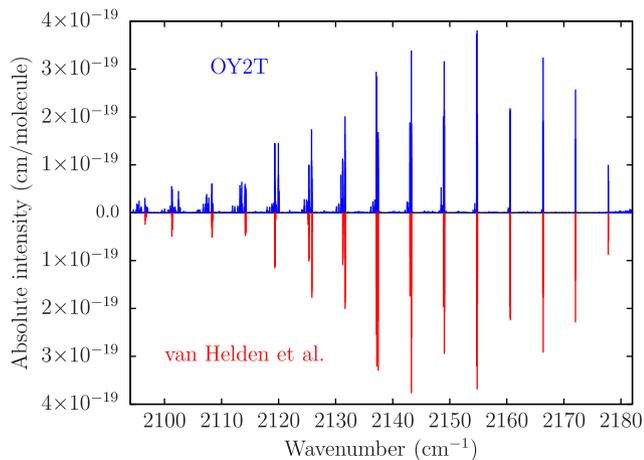

Figure 8. Absolute line intensities of the OY2T line list at $T = 296$ K compared with measurements from van Helden et al. (2015).
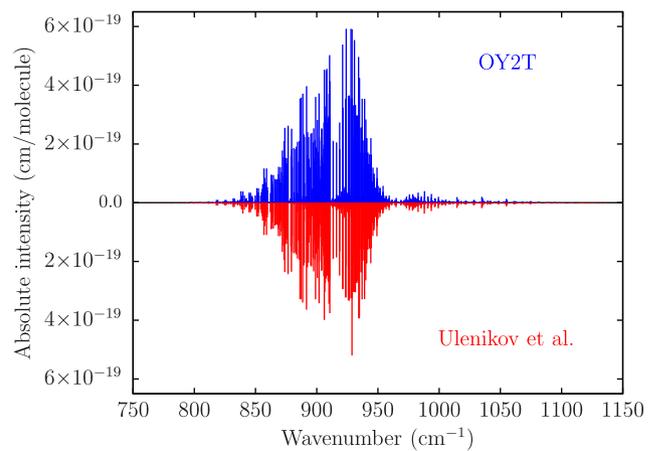

Figure 9. Absolute line intensities of the OY2T line list at $T = 298$ K compared with the line list from Ulenikov et al. (2017).

REFERENCES

Barber R. J., Tennyson J., Harris G. J., Tolchenov R. N., 2006, MNRAS, 368, 1087

Beaulieu J. P. et al., 2010, MNRAS, 409, 963

Beaulieu J. P. et al., 2011, ApJ, 731, 16

Boudon V., Rey M., Loëte M., 2006, J. Quant. Spectrosc. Radiat. Transf., 98, 394

Bunker P. R., Jensen P., 1998, Molecular Symmetry and Spectroscopy, 2nd edn. NRC Research Press, Ottawa

Canty J. I. et al., 2015, MNRAS, 450, 454

Chevalier M., 1988, Thesis, Université de Paris Sud, France

Cooley J. W., 1961, Math. Comput., 15, 363

Furtenbacher T., Császár A. G., 2012, J. Quant. Spectrosc. Radiat. Transf., 113, 929

Furtenbacher T., Császár A. G., Tennyson J., 2007, J. Mol. Spectrosc., 245, 115

Goldhaber D. M., Betz A. L., 1984, ApJ, 279, L55

Keady J. J., Ridgway S. T., 1993, ApJ, 406, 199

Larson H. P., Fink U., Smith H. A., Davis D. S., 1980, ApJ, 240, 327

Lin H., Wang D., Chen X. Y., Wang X. G., Zhou Z. P., Zhu Q. S., 1998, J. Mol. Spectrosc., 192, 249

Mizus I. I., Alijah A., Zobov N. F., Kyuberis A. A., Yurchenko S. N., Tennyson J., Polyansky O. L., 2017, MNRAS, 468, 1717

Monnier J. D., Danchi W. C., Hale D. S., Tuthill P. G., Townes C. H., 2000, ApJ, 543, 868

Neale L., Miller S., Tennyson J., 1996, ApJ, 464, 516

Noumerov B. V., 1924, MNRAS, 84, 592

Owens A., Yurchenko S. N., Yachmenev A., Thiel W., 2015, J. Chem. Phys., 143, 244317

Rey M., Nikitin A. V., Babikov Y. L., Tyuterev V. G., 2016, J. Mol. Spectrosc., 327, 138

Rivlin T., Lodi L., Yurchenko S. N., Tennyson J., Le Roy R. J., 2015, MNRAS, 451, 5153

Seager S., Bains W., Hu R., 2013, ApJ, 777, 95

Seager S., Bains W., Petkowski J. J., 2016, Astrobiology, 16, 465

Sharpe S. W., Johnson T. J., Sams R. L., Chu P. M., Rhoderick G. C., Johnson P. A., 2004, Appl. Spectrosc., 58, 1452

Snellen I., 2014, Phil. Trans. Royal Soc. London A, 372, 20130075

Steward W. B., Nielsen H. H., 1934, J. Chem. Phys., 2, 712

Steward W. B., Nielsen H. H., 1935, Phys. Rev., 47, 828

Sun F. G., Wang X. G., Zhu Q. S., Pierre C., Pierre G., 1995, Chem. Phys. Lett., 239, 373

Tennyson J., Yurchenko S. N., 2012, MNRAS, 425, 21

Tennyson J., Yurchenko S. N., 2017, Int. J. Quantum Chem., 117, 92

Tennyson J. et al., 2016, J. Mol. Spectrosc., 327, 73

Tinetti G. et al., 2007, Nature, 448, 169

Treffers R. R., Larson H. P., Fink U., Gautier T. N., 1978, Icarus, 34, 331

Tsiaras A. et al., 2016, ApJ, 820, 99

Tsiaras A. et al., 2017, ApJ, in press

Ulenikov O. N., Gromova O. V., Bekhtereva E. S., Raspopova N. I., Kashirina N. V., Fomchenko A. L., Sydow C., Bauerecker S., 2017, J. Quant. Spectrosc. Radiat. Transf., 196, 159

van Helden J. H., Lopatik D., Nave A., Lang N., Davies P. B., Röpcke J., 2015, J. Quant. Spectrosc. Radiat. Transf., 151, 287

Wenger C., Champion J. P., 1998, J. Quant. Spectrosc. Radiat. Transf., 59, 471

Yachmenev A., Yurchenko S. N., 2015, J. Chem. Phys., 143, 014105

Yurchenko S. N., Tennyson J., 2014, MNRAS, 440, 1649

Yurchenko S. N., Carvajal M., Jensen P., Herregodts F., Huet T. R., 2003, Chem. Phys., 290, 59

Yurchenko S. N., Thiel W., Jensen P., 2007, J. Mol. Spectrosc., 245, 126

Yurchenko S. N., Barber R. J., Yachmenev A., Thiel W., Jensen P., Tennyson J., 2009, J. Phys. Chem. A, 113, 11845

Yurchenko S. N., Barber R. J., Tennyson J., 2011, MNRAS, 413, 1828

Yurchenko S. N., Barber R. J., Tennyson J., Thiel W., Jensen P., 2011, J. Mol. Spectrosc., 268, 123

Yurchenko S. N., Tennyson J., Bailey J., Hollis M. D. J., Tinetti G., 2014, Proc. Natl. Acad. Sci. U.S.A., 111, 9379

Yurchenko S. N., Yachmenev A., Ovsyannikov R. I., 2017, J. Chem. Theory Comput., in press

Yurchenko S. N., Amundsen D. S., Tennyson J., Waldmann I. P., 2017, A&A, in press

Zhu Q. S., Qian H. B., Ma H., Halonen L., 1991, Chem. Phys. Lett., 177, 261

SUPPORTING INFORMATION

Supplementary data are available at *MNRAS* online.

Please note: Oxford University Press is not responsible for the content or functionality of any supporting materials supplied by the authors. Any queries (other than missing material) should be directed to the corresponding author for the article.

This paper has been typeset from a TeX/LaTeX file prepared by the author.